

Tuning of bound states in the continuum by waveguide rotation

Almas F. Sadreev, Artem S. Pilipchuk, and Alina A. Lyapina

Kirensky Institute of Physics, Federal Research Center KSC SB RAS, 660036 Krasnoyarsk, Russia

(Dated: March 3, 2022)

We consider acoustic wave transmission in non axisymmetric waveguide which consists of cylindrical resonator and two semi-infinite cylindrical waveguides whose axes are shifted relative to the resonator axis and each other by azimuthal angle $\Delta\phi$. We show that for rotation of one of attached waveguides the coupling matrix elements of the eigenmodes of resonator classified by the integer m and propagating mode of the waveguide acquire phase factor $e^{im\Delta\phi}$. That crucially effect Fano resonances and creates an analog of faucet opening and closing wave flux under rotation of the waveguide. We show that under the rotation of the waveguide and variation of the length of resonator numerous bound states in the continuum occur complimenting by the Fano resonance collapse.

I. INTRODUCTION

The beauty of complex wave fields observed in different areas of physics is related to the phase of the field. The first demonstration of the phase effect was done by Thomas Young in 1803 in the historic experiment on double-slit interference[1]. Among numerous phase features we mark bound states in the continuum (BSC) [2], Aharonov-Bohm oscillations [3], Fano asymmetric resonance [4], and topological singularities [5] which milestone the phase features in the last century. In the present paper we consider a waveguide setup which unites these features in wave transmission. The setup as shown in Fig. 1 consists of a cylindrical resonator of radius R and length L with two attached semi-infinite cylindrical waveguides. Tuning of the shape of the resonator could be performed in a realistic acoustic or electromagnetic experiment by the use of piston-like hollow-stem waveguides tightly fit to the interior boundaries of a cylindrical cavity [6] as shown in Fig. 1.

If the waveguides were attached coaxially the total system would be invariant relative to azimuthal rotation to split the total Hilbert space of the system into independent subspaces given by the orbital angular momentum (OAM) m . Respectively the wave transmission would take place independently in each sector given by the integer m with prohibition for OAM conversion. Variation of the resonator length rearranges the eigenlevels to allow for tuning Fano resonances which can be distinguished by changing the coupling strengths of the eigenmodes with the propagating modes of waveguide [7].

In the present paper we choose different strategy for tuning of Fano resonances based on an attachment of the phase to the coupling strengths by means of the rotation of one of the waveguides by the angle $\Delta\phi$ as shown in Fig. 1. Then one of the waveguides acquires phase difference relative to the other that crucially effects interference of resonances, i.e., the Fano resonances and the wave transmission. We show that even tiny rotations result in change of the transmittance from zero to the unit qualifying the setup as the wave faucet. Under variation of the resonator length multiple events of level crossing occur when the BSCs in the Friedrich-Wintgen scenario of wave localization through the full destructive interference of decaying resonant modes arise [8–10]. For coaxial attachment this scenario of the BSCs was considered in Ref. [6] in sector $m = 0$. Similar effects take place in sectors $m \neq 0$ with the BSCs degenerate with respect to the sign $\pm m$. Each BSC with $m \neq 0$ gives rise to flows of acoustic intensity spinning clockwise or anticlockwise inside the resonator. The importance of such spinning trapped modes in acoustics was first shown by Parker for axial flow compressor [11]. Their existence in a cylindrical acoustic infinitely long waveguide which contains rows of large numbers of blades arranged around a central core, was first reported by Duan and McIver [12]. The BSCs have become one of actively studied phenomena in different physical areas [13] because of potential applications in lasing [14, 15] and light enhancement in photonics [16–19]. Attachment of waveguides in non-coaxial manner breaks the azimuthal symmetry mixing all subspaces m in wave transmission. The most striking effect is that the evanescent modes of the waveguides lifts a degeneracy of the eigenlevels with respect to the sign of m . Then for arbitrary length of the resonator twist BSCs arise at selected angles $\Delta\phi_c$. Because of absence of the azimuthal symmetry such BSCs are not spinning.

II. WAVE FAUCET

In this section we consider wave transmission in dependence on angle $\Delta\phi$, the length of the resonator and frequency. For numerical simulations we employ the acoustic coupled mode theory which is in fact the effective non-Hermitian Hamiltonian approach [20, 21] adapted for the Neumann boundary conditions [22]. The propagating modes in sound

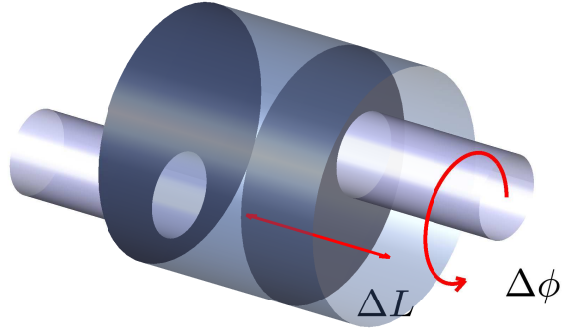


FIG. 1: (Color online) Cylindrical resonator of radius $R = 3$ and length L with two non-axially attached cylindrical waveguides of radius $r = 1$. The input waveguide can freely move along and rotate.

hard cylindrical waveguides are described by

$$\begin{aligned} \psi_{pq}(\rho, \alpha, z) &= \phi_{pq}(\rho) \frac{1}{\pi\sqrt{2k_{pq}}} e^{ip\alpha + ik_{pq}z}, \\ \phi_{0n}(\rho) &= \frac{1}{J_0(\mu_{0q})} J_0(\mu_{0q}\rho), \\ \phi_{pq}(\rho) &= \sqrt{\frac{1}{\mu_{pq}^2 - p^2}} \frac{\mu_{pq}}{J_p(\mu_{pq})} J_p(\mu_{pq}\rho) \quad , \end{aligned} \quad (1)$$

where ρ , α are the polar coordinates, μ_{pq} is the q -th root of equation $J'_p(\mu_{pq}\rho)|_{\rho=1} = 0$,

$$k_{pq}^2 = \omega^2 - \mu_{pq}^2 \quad (2)$$

The quantities ρ , z , k_{pq} are dimensionless via the radius of the waveguide. The frequency is measured in the units of the ratio of the sound velocity to the radius of the waveguides. Sound propagating bands are classified by two integers: the azimuthal number $p = 0, \pm 1, \pm 2, \dots$ and $q = 1, 2, 3, \dots$ with shapes of two degenerate transversal solutions $\cos p\alpha$ and $\sin p\alpha$ depicted in Table I.






The inner Hilbert space of the closed cylindrical resonator is spanned by the eigenmodes

$$\Psi_{mnl}(r, \phi, z) = \psi_{mn}(r) \sqrt{\frac{1}{2\pi}} \exp(im\phi) \psi_l(z), \quad (3)$$

where

$$\psi_{0n}(r) = \frac{\sqrt{2}}{R J_0(\mu_{0n})} J_0(\mu_{0n}r),$$

TABLE I: Propagating bands and corresponding radial eigenmodes $Re(\phi_p(r, \phi))$

Channel	Bottom of band	Indexes	mode shapes
1	0	$p = 0, q = 1$	
2	1.84118	$p = \pm 1, q = 1$	
3	3.0542	$p = \pm 2, q = 1$	
4	3.831706	$p = 0, q = 2$	
5	4.2012	$p = \pm 3, q = 1$	

$$\begin{aligned}\psi_{mn}(r) &= \sqrt{\frac{2}{\mu_{mn}^2 - m^2}} \frac{\mu_{mn}}{R J_m(\mu_{mn})} J_m(\mu_{mn} r / R), m \neq 0, \\ \psi_l(z) &= \sqrt{\frac{2 - \delta_{l,1}}{L}} \cos[\pi(l-1)z/L], l = 1, 2, 3, \dots\end{aligned}\quad (4)$$

$l = 1, 2, 3, \dots$ and z is measured in terms of the waveguide radius. The corresponding eigenfrequencies are

$$\omega_{mnl}^2 = \left[\frac{\mu_{mn}^2}{R^2} + \frac{\pi^2(l-1)^2}{L^2} \right] \quad (5)$$

where μ_{mn} is the n -th root of equation following from the Neumann boundary condition on the walls

$$J'_m(\mu_{mn} r)|_{r=R} = 0$$

Let us write the effective non-Hermitian Hamiltonian as [6, 22]

$$\widehat{H}_{eff} = \widehat{H}_R - i \sum_{C=L,R} \sum_{pq} k_{pq} \widehat{W}_C \widehat{W}_{C,pq}^\dagger \quad (6)$$

where \widehat{H}_R describes the closed resonator. The matrix elements of \widehat{W} are given by overlapping integrals [22, 23]

$$W_{mnl;pq}^C = \psi_l(z_C) \int_0^{2\pi} d\alpha \int_0^1 \rho d\rho \psi_{pq}(\rho, \alpha) \Psi_{mn}^*(r(\rho, \alpha), \phi(\rho, \alpha)) \quad (7)$$

where $z_C = 0, L$ are the position of the edges of the resonator along the z -axis. According to Eq. (3) we have

$$\psi_l(z=0) = \sqrt{\frac{2 - \delta_{l,1}}{L}}, \psi_l(z=L) = \psi_l(0)(-1)^{l-1}. \quad (8)$$

Integration is performed over circular cross section of the attached waveguides as shown in Fig. 2. According to Fig. 2 one can link the polar coordinates of the resonator with that of the waveguide

$$r \sin \phi = \rho \sin \alpha, r \cos \phi = r_0 + \rho \cos \alpha$$

where r_0 is the distance between the axes of the waveguide and resonator.

Although the waveguides are identical they are attached to the resonator at different azimuthal angles as shown in Fig. 2 to give rise to an exact relation between the coupling matrix elements

$$W_{mnl;pq}^R = (-1)^{l-1} e^{im\Delta\phi} W_{mnl;pq}^C \quad (9)$$

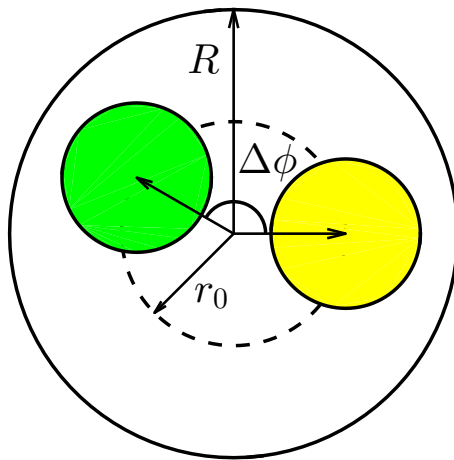


FIG. 2: (Color online) Filled areas show overlapping integration area in the coupling matrix (7).

Here $W_{mnl;pq} = W_{mnl;pq}^L$ are the coupling matrix elements of the resonator modes specified by integers m, n, l with p, q propagating modes of the left waveguide (see Fig. 1). Then the effective Hamiltonian takes the following form

$$\begin{aligned} \langle mnl | \hat{H}_{eff} | m'n'l' \rangle &= \omega_{mnl}^2 \delta_{mm'} \delta_{nn'} \delta_{ll'} \\ &- i \sum_{pq} k_{pq} [1 + (-1)^{l+l'} e^{i(m-m')\Delta\phi}] W_{mnl;pq} W_{m'n'l';pq}^* \end{aligned} \quad (10)$$

The transmittance of sound waves through the resonator is given by the inverse of the matrix $\hat{G} = \hat{H}_{eff} - \omega^2$ [20, 22]

$$T_{pq;p'q'} = -2ik_{pq} \sum_{mnl} \sum_{m'n'l'} W_{mnl;pq} \langle mnl | [\hat{H}_{eff} - \omega^2]^{-1} e^{i(m-m')\Delta\phi} | m'n'l' \rangle W_{m'n'l';p'q'}^* \quad (11)$$

In what follows we take both waveguides with unit radius shifted relative to the central axis of the resonator with the radius $R = 3$ by a distance $r_0 = 1.5$. We consider transmission in the first channel $p = 0, q = 1$ in the frequency domain $0 < \omega < 1.8412$ as shown in Table I. The transmittance versus the squared frequency and the resonator length L shown in Fig. 3 (a) and (b) for $\Delta\phi = 0, \pi/4$ respectively. The resonant behavior of the transmittance is due to that the resonator is three-dimensional. The coupling matrix elements (7) can be estimated as the ratio of the cross-section of the waveguides to the cross-section of the resonator. The resonant widths are proportional to squared coupling matrix elements, i.e., proportional to R^{-4} , while the distance between the eigenlevels is proportional to $\Delta E \sim R^{-2}$. Hence for $R = 3$ we have the regime of weak coupling [25] while for two-dimensional resonator one would have $\Gamma \sim R^{-2}$ as well as $\Delta E \sim R^{-2}$, i.e., the regime of overlapping resonances [6]. In the two-dimensional systems the regime of weak coupling can be reached only by use of special diaphragms [7]. Indeed Fig. 3 (a) and (b) shows that the transmittance of the resonator basically follows the eigenvalues of the closed resonator.

When $\Delta\phi \neq 0$ the transmittance undergoes changes in the vicinity of eigenvalue crossings as shown in Fig. 3 (b). Figs. 3 (c) and 3 (d) brightly demonstrate the effect of wave faucet when the resonator is opened or closed by rotation of the waveguide. The features of wave interference under rotation of the waveguide are demonstrated in Figs. 4, 5, and 6 where the transmittance is shown in higher resolution in zoomed windows. First of all one can see a high sensitivity of the transmittance to the rotation angle $\Delta\phi$. Moreover there are a mass of points in the vicinity of which even extremely small changes in parameters of the system cause drastic changes in the transmittance. These points are marked by open circles and correspond to the BSCs. In the vicinity of the BSC points the unit transmittance coalesces with zero transmittance (collapse of the Fano resonance [10, 38]). In particular, one can see in Fig. 5 that even the slightest rotation opens and closes the resonator illustrating the effects of wave faucet. These resonant angular features are the result of evanescent modes and will be studied analytically by use of truncated effective Hamiltonian.

III. BOUND STATES IN THE CONTINUUM

In Figs. 3, 4 and 5 we show BSC points by closed and open circles. The procedure to find BSCs is based on search of real eigenvalues of the effective non-Hermitian Hamiltonian (6) $z_\lambda(\omega, L, \Delta\phi)$ [24]. A typical behavior of the

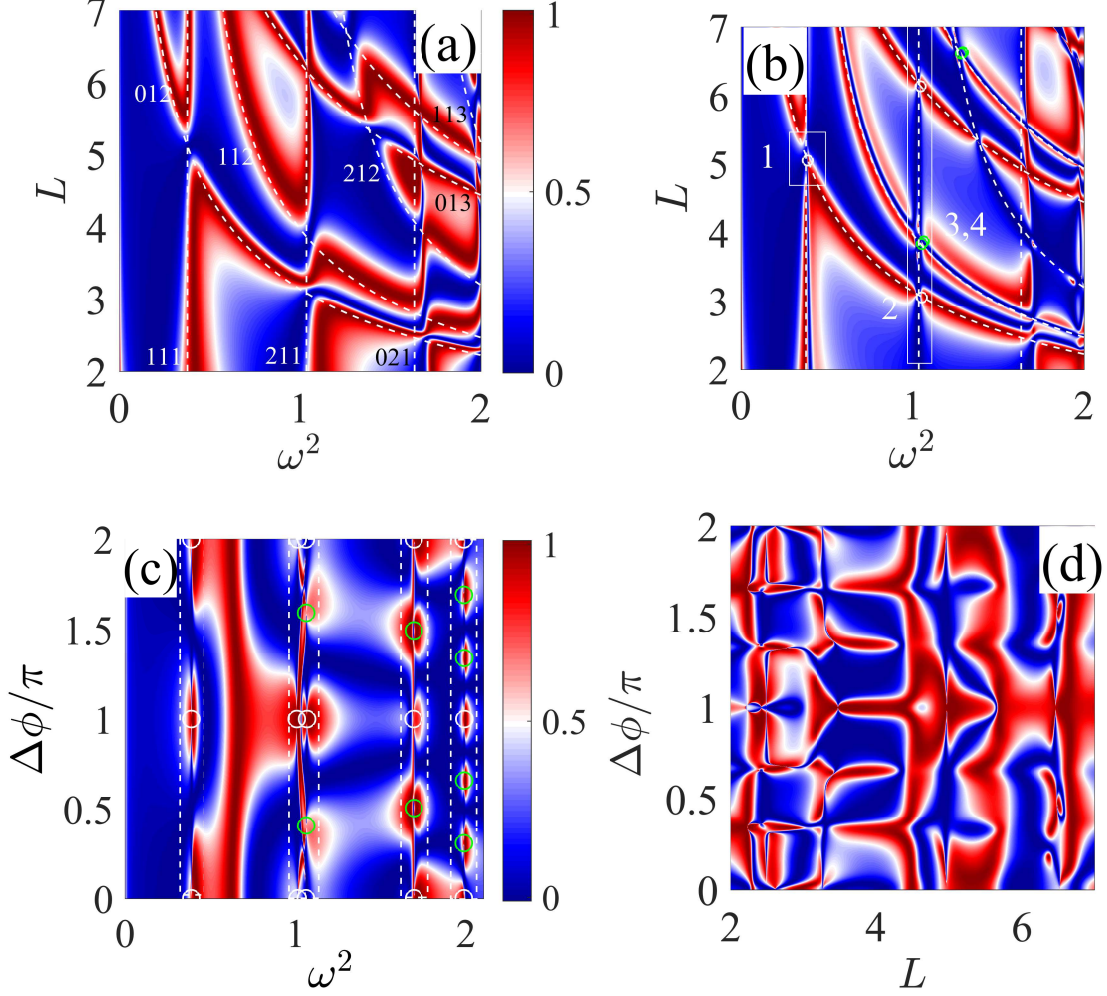


FIG. 3: (Color online) Transmittance of a cylindrical resonator vs frequency and length of the resonator L at (a) $\Delta\phi = 0$ and (b) $\Delta\phi = \pi/4$. (c) vs frequency and rotation angle $\Delta\phi$ at $L = 4$ and (d) vs length and rotation angle at $\omega^2 = 2$. Dash lines in (a) show eigenfrequencies of closed resonator with corresponding indexes mnl . The positions of the BSCs are shown by closed circles.

imaginary parts (resonant widths) as dependent on the length L (a) and rotation angle $\Delta\phi$ (b) is shown in Fig. 6. One can see numerous events of turning of resonant widths to zero. Each BSC point is searched by solving the fix point equations [20] $\omega = \text{Re}(z(\omega, L, \Delta\phi))$, $\text{Im}(z(\omega, L, \Delta\phi)) = 0$. After the fix point equation is solved we can determine the eigenmodes of the effective Hamiltonian with real eigenvalues which are BSC mode shapes [6, 10]. Fig. 7 shows the expansion coefficients a_{mnl} of the BSCs over the eigenmodes of the closed resonator (3)

$$\psi_{BSC}(r, \phi, z) = \sum_{mnl} a_{mnl} \Psi_{mnl}(r, \phi, z). \quad (12)$$

The expansion coefficients a_{mnl} are listed in Table II for the BSCs enumerated from one to four in Fig. 3 (a).

From Fig. 3 (a), (b) and Fig. 4 one can see that the BSCs are positioned in the vicinity of degeneracy points. However one can see from Fig. 4 (a) that the BSC 1 are not spaced exactly at the degeneracy point of eigenlevels 012 and ± 111 due to the evanescent modes [10]. The second feature of the BSCs is the frequency splitting in the vicinity of the crossing of eigenlevels with $m = \pm 1$ and $m = \pm 2$. Such split BSCs 3 and 4 are shown by closed circles in Fig. 4 (b). Fig. 7 shows that the BSCs are composed of the eigenmodes of the closed resonator $\Psi_{mnl}(r, \phi, z)$ which undergo degeneracy in the vicinity of the BSC point. Surprisingly, although BSCs are superposed of complex functions $e^{im\phi}$ they do not support flows of acoustic intensity in contrast to the case of coaxial attachment of waveguides [12]. As Fig. 7 shows each pair of eigenmodes with $\pm m$ contributes into the BSC with equal $|a_{mnl}|$.

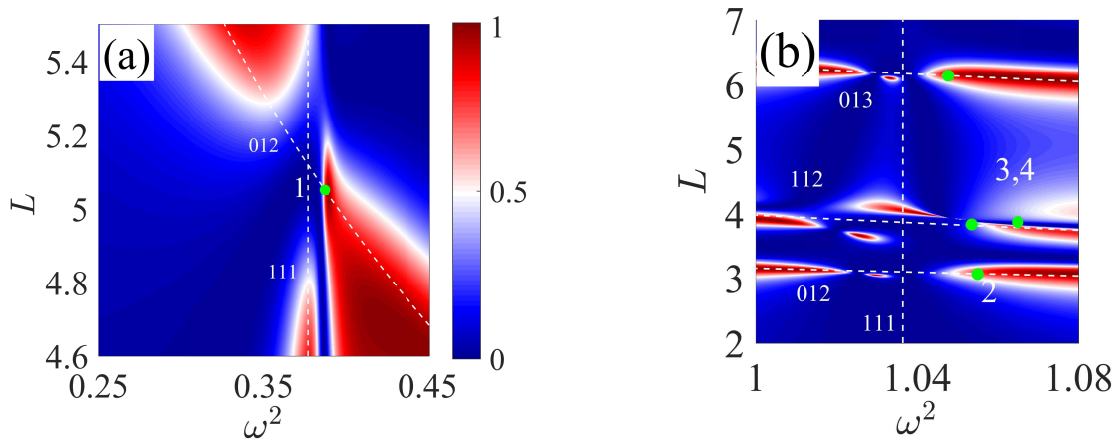


FIG. 4: (Color online) Transmittance vs frequency and length at $\Delta\phi = \pi/4$ at $L = 4$ in the domains shown in Fig. 3 (b) by rectangles.

TABLE II: BSC points and their expansion coefficients a_{mnl} .

BSC number	ω^2	L	$\Delta\phi$	mnl	a_{mnl}
1	0.385	5.065	$\pi/4$	012	$-0.113+0.272i$
				111	$-0.478(1-i)$
				-111	0.675
2	1.055	3.051	$\pi/4$	012	$-0.261(1-i)$
				211	0.656i
				-211	0.656
3	1.0535	3.833	$\pi/4$	211	0.658i
				-211	0.658
				112	$-0.237-0.098i$
				-112	$-0.098-0.237i$
4	1.065	3.869	$\pi/4$	211	-0.505
				-211	0.505
				112	$-0.455-0.189$
				-112	$0.189+0.455i$

IV. BSCS IN TWO CONTINUA DIFFERENT IN PHASE

Displacement of the waveguide relative to the resonator does not change its continuous spectrum. However the coupling matrix elements of the resonator eigenmodes with the continua are subject to alternation to affect the transmission. In particular under rotation of one of the waveguides the matrix elements acquire phase shift (9). Therefore in the framework of the effective non-Hermitian Hamiltonian one can say that two continua become different by phase. First, the problem of the BSC residing in a finite number of continua was considered by Pavlov-Verevkin and coauthors [28]. Rigorous statement about the BSCs was formulated as follows. The interference among N degenerate states which decay into K non-interacting continua generally leads to the formation of $N - K$ BSCs. The equivalent point of view [10, 30] is that the linear superposition of the N degenerate eigenstates $\sum_{n=1}^N a_n \psi_n$ can be adjusted to have zero coupling with K different continua in $N - K$ ways by variation of the N superposition coefficients a_n . Respectively, these coefficients a_n define an expansion of the BSC over the eigenstates of the closed resonator. The number of continua can grow due to a number of reasons, for example, non-symmetrically attached waveguides, multiple propagation subbands in the waveguides, or two polarizations of the radiation continuum in case of electromagnetic BSCs. Each case puts the problem of constructing BSCs in the case of many continua on the line of art [18, 30–34].

In the present case of waveguide rotation the number of continua has been doubled for the frequency of sound waves below the second propagation threshold $\omega < \mu_{11}$ (see Table I). Therefore we could expect BSCs only at the points of threefold degeneracy in compliance with the generic statement [28]. There are indeed numerous points

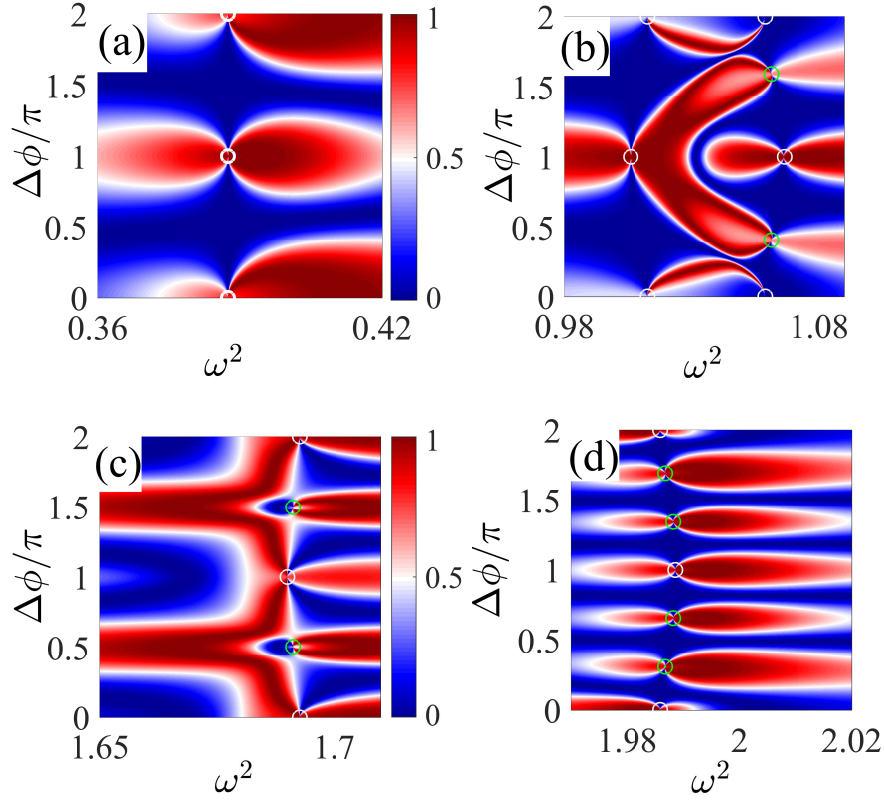


FIG. 5: (Color online) Transmittance vs frequency and rotation angle $\Delta\phi$ at $L = 4$ in frequency domains shown in Fig. 3 (c) by dash rectangles. The positions of the BSCs are shown by closed circles.

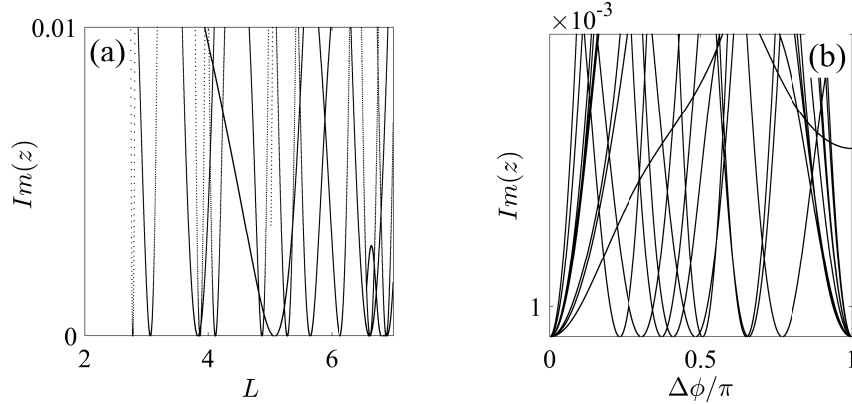


FIG. 6: (Colour online) Evolution of resonant widths under variation of (a) the resonator length at $\Delta\phi = \pi/4$ and (b) rotation of the waveguide at $L = 4$.

where the eigenlevels ω_{mnl}^2 double degenerate in $\pm m$ cross the eigenlevels ω_{0nl}^2 with BSCs marked by open circles in Fig. 3 (b) and (c). However the zoomed picture of transmission in Fig. 4 (a) shows that this conclusion is only approximate. Thus, the case needs in special consideration. As shown in Table II the BSCs are superposed from only a few eigenmodes. Hence we can truncate the effective Hamiltonian to the relevant eigenmodes similar to that in Refs. [8–10].

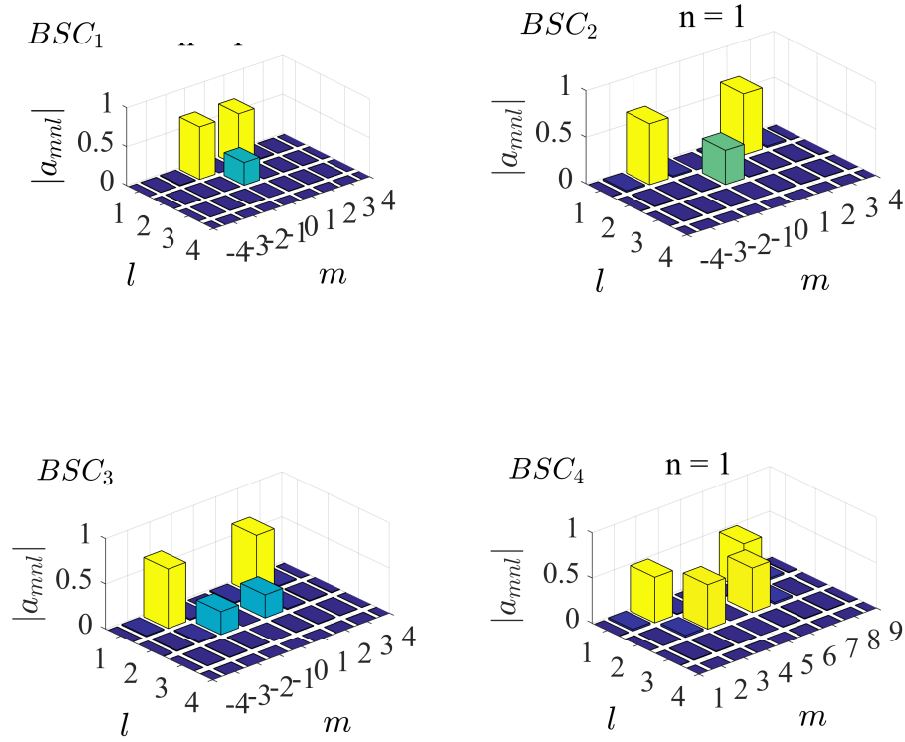


FIG. 7: (Color online) Modal expansion coefficients $|a_{mnl}|$ of BSCs shown in Fig. 3 for the case $\Delta\phi = \pi/4$.

A. The mode with $m = 0$ crosses the modes with $\pm m$

Let us consider the crossing of the eigenlevel $\omega_{012}^2 = \pi^2/L^2$ with the degenerate eigenlevel $\omega_{111}^2 = \mu_{11}^2/R^2$ shown in Fig. 8 by dash lines. The coupling matrix elements of the eigenmodes with the first propagating channel $p = 0, q = 1$

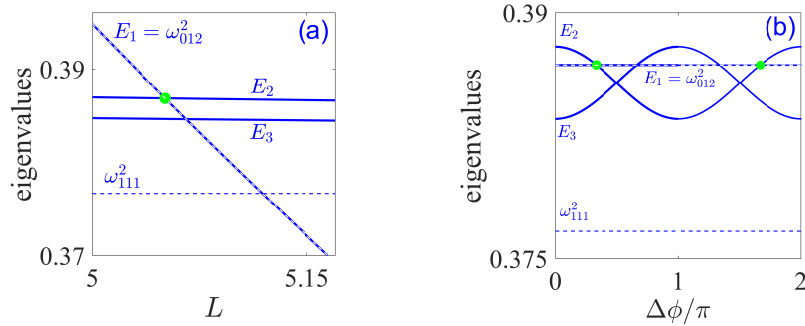


FIG. 8: (Color online). The eigenvalues of the closed resonator (dash lines) and the eigenlevels (19) (solid lines) shifted by evanescent modes vs (a) the resonator length at $\phi = \pi/3$ and (b) rotation angle at $L = 5.0512$.

(see Table I) of the right waveguide according to Eqs. (1), (4) and (7) equal

$$\begin{aligned}
 W_{mnl;01} &= (w_0 \ w_1 \ w_1), w_0 = W_{012;01} = \frac{1}{3}\sqrt{\frac{2}{L}}, \\
 w_1 &= W_{\pm 111;01} = 0.269\sqrt{\frac{1}{L}}
 \end{aligned} \tag{13}$$

for the given radius of the resonator. We also take into account the coupling with the first evanescent modes $p = \pm 1, q = 1$ of the waveguide (see Table I)

$$\begin{aligned} W_{mnl;11} &= (0 \ v_1 \ v_2), \quad W_{mnl;-11} = (0 \ v_2 \ v_1), \\ v_1 &= W_{012;11}^L = 0.1141\sqrt{\frac{1}{L}}, \quad v_2 = W_{\pm 111;11} = -0.0141\sqrt{\frac{1}{L}}. \end{aligned} \quad (14)$$

Because of the phase difference between the coupling matrix elements for left and right waveguides we immediately obtain

$$\begin{aligned} W_{mnl;01}^R &= (-w_0 \ w_1 e^{i\Delta\phi} \ w_1 e^{-i\Delta\phi}), \\ W_{mnl;11}^R &= (0 \ v_2 e^{i\Delta\phi} \ v_1 e^{-i\Delta\phi}), \\ W_{mnl;-11}^R &= (0 \ v_1 e^{i\Delta\phi} \ v_2 e^{-i\Delta\phi}). \end{aligned} \quad (15)$$

The contribution of the higher evanescent modes shown in Table I is negligible. For open channel $p = 0, q = 1$ the wave number $q_{01} = \omega$ while for the next closed channel $p = \pm 1, q = 1$ the wave number $k_{11} = iq_{11}, q_{11} = \sqrt{\mu_{11}^2 - \omega^2}$ is imaginary. Then the truncated effective Hamiltonian (6) can be rewritten as follows

$$\hat{H}_{eff} = \hat{H}_R + q_{11} \sum_{C=L,R} \sum_{p=\pm 1} \widehat{W}_{p=\pm 1,1}^C \{\widehat{W}_{p=\pm 1,1}^C\}^\dagger - i\omega \sum_{C=L,R} \widehat{W}_{01}^C \{\widehat{W}_{01}^C\}^\dagger = \widehat{\widetilde{H}}_R - i\omega \widehat{\Gamma}, \quad (16)$$

where the Hermitian term

$$\widehat{\widetilde{H}}_R = \begin{pmatrix} \omega_{012}^2 & 0 & 0 \\ 0 & \omega_{111}^2 + 2q_{11}(v_1^2 + v_2^2) & 2q_{11}v_1v_2(1 + e^{-2i\Delta\phi}) \\ 0 & 2q_{11}v_1v_2(1 + e^{2i\Delta\phi}) & \omega_{111}^2 + 2q_{11}(v_1^2 + v_2^2) \end{pmatrix} \quad (17)$$

is the Hamiltonian of the resonator coupled to the evanescent modes. The anti-Hermitian part takes the following form

$$\widehat{\Gamma} = \begin{pmatrix} 2w_0^2 & w_0w_1(1 - e^{i\Delta\phi}) & w_0w_1(1 - e^{-i\Delta\phi}) \\ w_0w_1(1 - e^{-i\Delta\phi}) & 2w_1^2 & w_1^2(1 + e^{-2i\Delta\phi}) \\ w_0w_1(1 - e^{i\Delta\phi}) & w_1^2(1 + e^{2i\Delta\phi}) & 2w_1^2 \end{pmatrix}. \quad (18)$$

The eigenvalues of the Hamiltonian (17) can be easily found as

$$E_1 = \omega_{012}^2, E_{2,3} = \omega_{111}^2 + 2q_{11}[v_1^2 + v_2^2 \pm 2v_1v_2 \cos \Delta\phi]. \quad (19)$$

Thus the evanescent modes of the waveguides non-coaxially attached to the cylindrical resonator lift the degeneracy of eigenmodes ± 111 as shown in Fig. 8 by solid lines. The only case when the degeneracy is restored is the case $\Delta\phi = \pi/2$. The corresponding eigenmodes of the Hamiltonian (17) are the following

$$\mathbf{X}_1 = \begin{pmatrix} 1 \\ 0 \\ 0 \end{pmatrix}, \mathbf{X}_2 = \frac{1}{\sqrt{2}} \begin{pmatrix} 0 \\ -e^{-i\Delta\phi} \\ 1 \end{pmatrix}, \mathbf{X}_3 = \frac{1}{\sqrt{2}} \begin{pmatrix} 0 \\ e^{-i\Delta\phi} \\ 1 \end{pmatrix}. \quad (20)$$

Next, let us consider the BSC in the truncated version (16). The point of the BSC can be easily diagnosed by zero resonant width as shown in Fig. 9. For $\Delta\phi = \pi/4$ the BSC occurs at $L = L_c = 5.0512$ marked by closed green circle in Fig. 9 (a). Respectively at $L = L_c$ the BSC occurs at $\Delta\phi = \pi/4$ and $\Delta\phi = 2\pi - \pi/4$. These points are seen in zoomed insert in Fig. 9 (b).

For $\Delta\phi = 0$ both continua of left and right waveguides coincide to result in the symmetry protected BSC superposed of degenerate eigenmodes of the closed resonator ψ_{111} and ψ_{-111} to be in the following form

$$\psi_{BSC}(r, \phi, z) = AJ_1(\mu_{11}r) \sin(\pi z/L) \sin \phi \quad (21)$$

which always has zero coupling with the propagation mode $\psi_{01}(\rho, \alpha, z)$ shown in Table I. As seen from Eq. (21) this conclusion also holds true for $\Delta\phi = \pi$. This BSC is symmetry protected for arbitrary resonator length as shown in Figs. 9, 12, and 13.

As soon as $\Delta\phi \neq 0$ the continua become different to destroy the symmetry protected BSCs. It could be expected that in the case of two waveguides the point of threefold degeneracy where the ω_{012} crosses the double degenerate ω_{111}

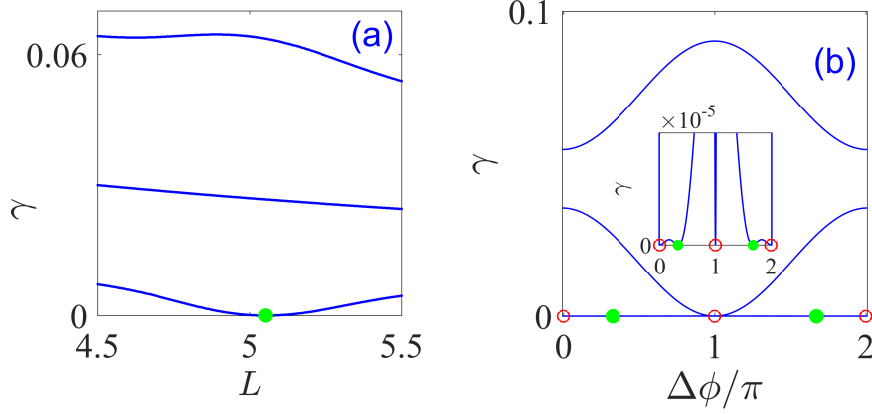


FIG. 9: (Color online). The resonant width vs (a) the resonator length at $\Delta\phi = \pi/3$ and (b) rotation angle at $L = 5.0512$. Circles show the BSC points.

as shown in Fig. 8 (a) is a BSC point in accordance with the above consideration. However the BSC point where the resonant width turns to zero (see Fig. 9) does not coincide with this point. The computation on the basis of full basis effective Hamiltonian gives the same result. In fact, the evanescent modes split the eigenvalues (19). Respectively the point of threefold degeneracy $\omega_{111}^2 = \omega_{012}^2(L)$ splits into two double degenerate points $E_1(L) = E_2(L, \Delta\phi)$ and $E_1(L) = E_3(L, \Delta\phi)$. As shown in Fig. 8 (a) the first case exactly corresponds to the BSC point but not the second.

In the first case we can superpose the eigenmodes (20) as $a\mathbf{X}_1 + b\mathbf{X}_2$ and require zero coupling of this superposed mode with the left waveguide

$$aw_0 + \frac{b}{\sqrt{2}}w_1(1 - e^{-i\Delta\phi}) = 0 \quad (22)$$

according to Eqs. (13) and (20). It is easy to show that the coupling with the phase shifted continuum of the left waveguide takes the *same* form as Eq. (22). Thus, the BSC has the following form

$$\psi_{BSC} = w_1(1 - e^{-i\Delta\phi})\psi_{012} + w_0(e^{-i\Delta\phi}\psi_{111} - \psi_{-111}). \quad (23)$$

Substituting eigenmodes (4) we obtain

$$\psi_{BSC} = 2ie^{-i\Delta\phi/2}[w_1 \sin(\Delta\phi/2)\psi_{01}(r)\psi_2(z) + w_0 \sin(\phi - \Delta\phi/2)\psi_{11}(r)\psi_1(z)]. \quad (24)$$

One can see that this BSC does not support spinning currents of acoustic intensity $\vec{j} = \psi^*\nabla\psi$ in contrast to coaxial waveguides [12]. This is due to evanescent modes of the non-coaxial waveguides which lift the degeneracy of the eigenmodes Ψ_{mnl} with respect to the sign m .

The BSC point is given by the equation $E_1(L) = E_2(L, \Delta\phi)$ which gives rise to a line of the BSC in the parametric space L and $\Delta\phi$ shown in Fig. 10. Thus, the only phase difference between the continua allow the BSCs in the point of twofold degeneracy. This is necessary for existence of BSC but not sufficient. Indeed let us consider the another point of degeneracy $E_1 = E_3$ (see Fig. 8 (a)). At this point we adjust the superposition $a\mathbf{X}_1 + b\mathbf{X}_3$ for cancellation of the coupling with both continua. The analogue of Eq. (22) takes the following form

$$\pm aw_0 + \frac{b}{\sqrt{2}}w_1(1 + e^{i\Delta\phi})w_1 = 0. \quad (25)$$

These equations can not be fulfilled simultaneously to forbid this degeneracy point as the BSC point.

By the use of Eq. (11) and truncated effective Hamiltonian (16) we calculated the transmittance with the results presented in Fig. 11. Comparison to Fig. 3 (a) and (b) shows that all features of the transmittance can be well reproduced in the vicinity of the BSCs by the use of truncated basis. One can also see from Fig. 11 that the resonant features follow the real parts of the complex eigenvalues of the effective non-Hermitian Hamiltonian (16) when $\Delta\phi \neq 0$.

Fig. 12 shows fine features of the transmittance vs two parameters for the third parameter exactly tuned to the BSC. Fig. 12 (a) demonstrates a Fano resonance collapse in the parametric space of length and rotation angle at the

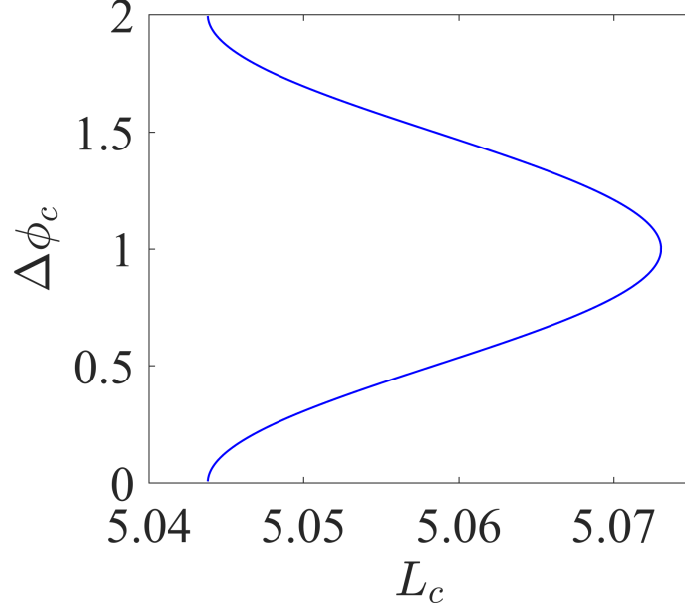


FIG. 10: (Color online) Line of the BSCs in the parametric space of the resonator length and rotation angle $\Delta\phi$.

BSC point $L_c = 5.048$ and $\Delta\phi_c = \pi/4$ with the frequency exactly tuned to the BSC $\omega_c = 0.3873$. Fig. 12 (b) shows the transmittance vs the frequency and the rotation angle for the length of the resonator tuned to the BSC length $L_c = 5.0584$. Fig. 12 (a) and Fig. 12 (b) show that the resonator is blocked when $\Delta\phi = 0$ and open when $\Delta\phi = \pi$. Fig. 13 demonstrates as the transmittance is sensitive to small deviations from the BSC length L_c .

One can see from Eqs. (13) and (15) that at $\Delta\phi = 0$ the channels 012 and ± 111 interfere destructively at the right output to block the wave transmission through the resonator. In contrast for $\Delta\phi = \pi$ the channels interfere constructively at the right output to maximize the transmittance. Along the same line for the channels 012 and ± 211 the wave faucet will open at $\Delta\phi = \pi/2, 3\pi/2$ because of the phase factor $e^{\pm 2i\Delta\phi}$ in the coupling matrix elements (15). Respectively, interference of channels of 013 and ± 211 will realize the wave faucet which opens at $\Delta\phi = 0, \pi$. Fig. 14 completely confirms the above predictions.

B. The mode ± 112 crosses the mode ± 211

The coupling matrix elements of the eigenmodes with the first propagating channel $p = 0, q = 1$ (see Table I) of the right waveguide according to Eqs. (1), (4), and (7) equal

$$\begin{aligned} W_{mnl;01}^R &= (w_1 \ w_1 \ w_2 \ w_2), w_1 = W_{211;01}^R = 0.1737\sqrt{\frac{1}{L}}, \\ w_2 &= W_{\pm 112;01}^R = 0.2849\sqrt{\frac{2}{L}}. \end{aligned} \quad (26)$$

The coupling matrix elements with the first evanescent modes $p = 1, n = 1$ of the left waveguide (see Table I) equal

$$\begin{aligned} W_{mnl;-11}^L &= (v_1 \ v_2 \ v_3 \ v_4), W_{mnl;11}^L = (v_2 \ v_1 \ v_4 \ v_3), \\ v_1 &= W_{-211;11}^L = 0.2197\sqrt{\frac{1}{L}}, v_2 = W_{211;11}^L = -0.0187\sqrt{\frac{1}{L}}, \\ v_3 &= W_{-112;11}^L = 0.1709\sqrt{\frac{2}{L}}, v_4 = W_{112;11}^R = -0.0157\sqrt{\frac{2}{L}}. \end{aligned} \quad (27)$$

Respectively according to Eq. (9) we have for the phase shifted coupling matrix elements $W_{mnl;pq}^R = V_{mnl}W_{mnl;pq}^L$. The resulting effective non-Hermitian Hamiltonian (6)

$$\hat{H}_{eff} = \hat{H} - i\omega\hat{\Gamma}$$

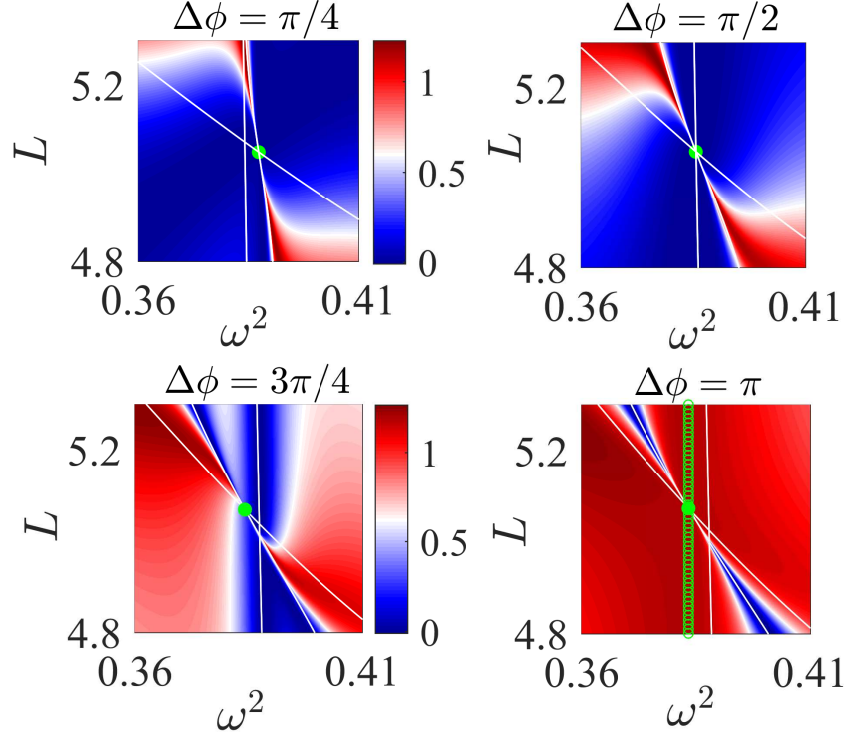


FIG. 11: (Color online) (a) Transmittance vs frequency and resonator length at four fixed rotation angles. Solid green lines show the resonances defined by real part of the complex eigenvalues of the effective Hamiltonian (16). Closed circles mark the BSCs which exactly correspond to points of degeneracy of the eigenlevels (19).

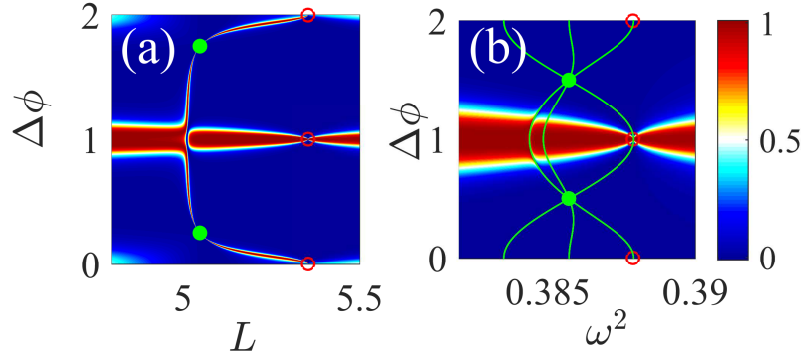


FIG. 12: (Color online) (a) Transmittance vs the resonator length and rotation angle for the frequency tuned onto the frequency of the BSC $\omega_c^2 = 0.388$. (b) Transmittance vs the frequency and rotation angle for the length tuned onto the BSC length $L_c = 5.048$. Closed circles mark BSC 1 resulted by crossing of eigenlevels (19) E_1 and E_2 , open circles mark the symmetry protected BSCs (21).

consists of

$$\widehat{H} = q_{11} \begin{pmatrix} \omega_{211}^2/q_{11} + 2v_1^2 & v_1v_2(1 + e^{4i\Delta\phi}) & v_1v_3(1 - e^{-i\Delta\phi}) & v_1v_4(1 - e^{-3i\Delta\phi}) \\ v_1v_2(1 + e^{-4i\Delta\phi}) & \omega_{211}^2/q_{11} + 2v_2^2 & v_2v_3(1 - e^{3i\Delta\phi}) & v_1v_4(1 - e^{i\Delta\phi}) \\ v_1v_3(1 - e^{i\Delta\phi}) & v_2v_3(1 - e^{-3i\Delta\phi}) & \omega_{112}^2/q_{11} + 2v_3^2 & v_3v_4(1 + e^{-2i\Delta\phi}) \\ v_1v_4(1 - e^{3i\Delta\phi}) & v_2v_4(1 - e^{-4i\Delta\phi}) & v_3v_4(1 + e^{2i\Delta\phi}) & \omega_{112}^2/q_{11} + 2v_4^2 \end{pmatrix} \quad (28)$$

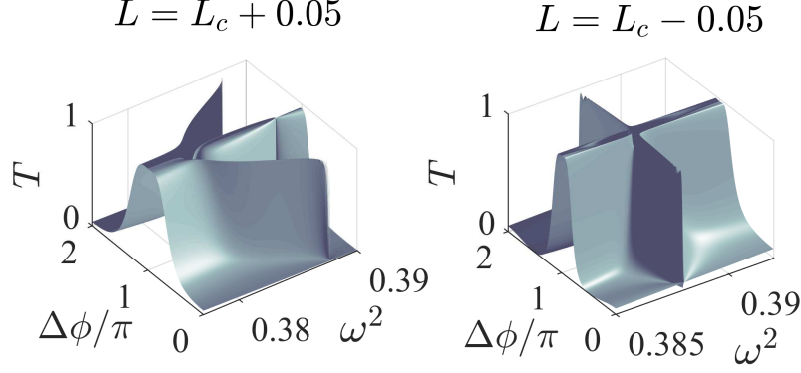


FIG. 13: (Color online) Transmittance vs the frequency and rotation angle for the length detuned from the BSC length L_c .

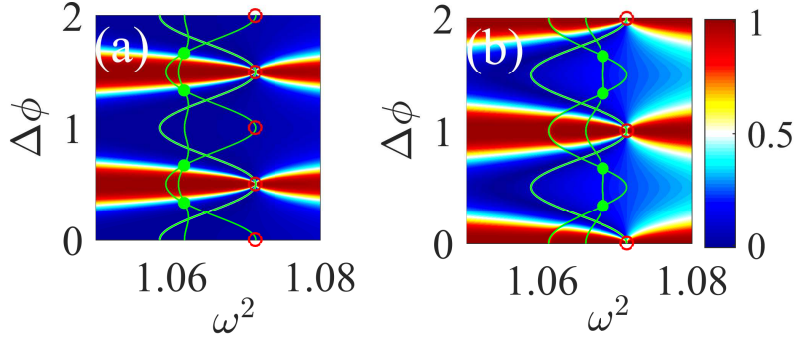


FIG. 14: (Color online) Transmittance vs the frequency and rotation angle in the vicinity of crossing of the modes (a) 012 and 211 at $L = 3$ and (b) 013 and 211, $L = 4$.

and

$$\hat{\Gamma} = \begin{pmatrix} 2|w_1|^2 & w_1^2(1 + e^{4i\Delta\phi}) & w_1w_2(1 - e^{-i\Delta\phi}) & w_1w_2(1 - e^{-3i\Delta\phi}) \\ w_1^2(1 + e^{-4i\Delta\phi}) & 2w_1^2 & w_1w_2(1 - e^{3i\Delta\phi}) & w_1w_2(1 - e^{i\Delta\phi}) \\ w_1w_2(1 - e^{i\Delta\phi}) & w_1w_2(1 - e^{-3i\Delta\phi}) & 2w_2^2 & w_2^2(1 + e^{-2i\Delta\phi}) \\ w_1w_2(1 - e^{3i\Delta\phi}) & w_1w_2(1 - e^{-i\Delta\phi}) & w_2^2(1 + e^{2i\Delta\phi}) & 2w_2^2 \end{pmatrix}. \quad (29)$$

In contrast to the previous case of crossing of eigenlevels 112 and 012 (the BSC 1), the present case of full matrices impedes analytical consideration of the BSCs. Nevertheless the small size of matrices (28) and (29) facilitates numerical treatment of the BSCs. Fig. 15 shows the eigenlevels of the Hamiltonian (28)

$$\hat{H}\mathbf{X}_j = E_j\mathbf{X}_j \quad (30)$$

as dependent on the length and rotation angle. One can see that the presence of evanescent modes lifts the degeneracy relative to the sign of m . Below in Fig. 15 we show the resonant widths that demonstrates two BSCs at the points: 1) $L_c = 3.7947, \omega_c^2 = 1.0756, \phi_c = \pi/4$ and 2) $L_c = 3.9312, \omega_c^2 = 1.0946, \phi = \pi/4$. Respectively, in Fig. 15 (b) we show the eigenvalues for these BSC lengths.

While the former BSCs occur at the crossing of eigenlevels (19) the present BSCs are allocated neither at the crossing of neither the eigenfrequencies ω_{112} and ω_{211} nor the eigenlevels modified by the evanescent modes as seen from Fig. 15. Such phenomenon is generic in open chaotic billiards where the eigenlevels of the closed billiard undergo avoided crossing [39] similar to that shown in Fig. 15 (a). In that case some of the eigenmodes of the Hamiltonian (28) can decouple under the evolution of the parameters of the resonator. In the truncated description of the BSCs

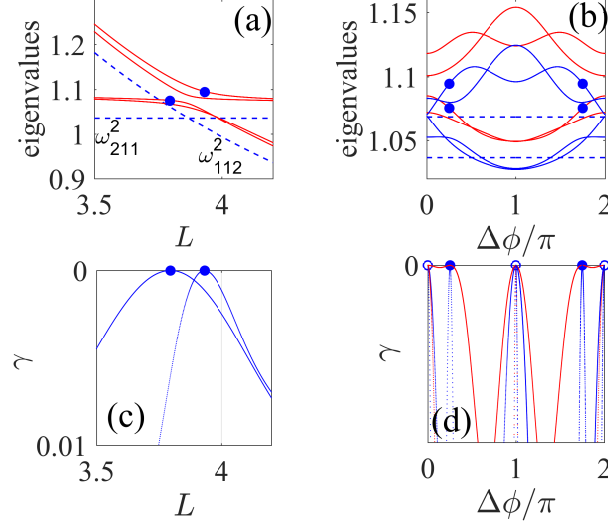


FIG. 15: (Color online) The eigenlevels (15) (solid lines) as dependent on (a) length of resonator at $\phi = \pi/41$ and (b) rotation angle at $L = 3.7947$ (blue) and $L = 3.9312$ (green) compared to the eigenfrequencies of the closed resonator (dash lines). (c) and (d) Corresponding behavior of the resonant widths defined by imaginary parts of the effective non-Hermitian Hamiltonian (28) and (29). Closed circles mark the BSCs. Open circles mark the symmetry protected BSCs.

TABLE III: BSC solutions 3 and 4 resulted by crossing of modes ± 112 and ± 211 .

BSC number	ω^2	L	$\Delta\phi$	mnt	a_{mnt}
3	1.0756	3.7947	$\pi/4$	211	0.6715i
				-211	0.6715
				112	-0.2047-0.0848i
				-112	-0.0848-0.2047i
4	1.0966	3.9312	$\pi/4$	211	-0.553i
				-211	0.553
				112	-0.407-0.168i
				-112	0.168+0.407i

we obtain the following solutions for the BSCs presented in Table III. Comparison with numerical results in full basis (Table II) shows good agreement with the BSCs (2) and (3). Anyway as seen from Fig. 7 the BSCs are expanded over all four eigenmodes ± 211 and ± 112 of the closed resonator. Remarkably, in the description of the eigenmodes (30) \mathbf{X}_j we obtain that the numerical amplitudes of the BSC mode $\psi_{BSC} = \sum_{j=1}^4 b_j \mathbf{X}_j$ are the following

$$\begin{aligned}
 (3) \quad \psi_{BSC} &= \mathbf{X}_2, \quad L_c = 3.7947, \quad \omega_c^2 = 1.0756, \quad \Delta\phi_c = \pi/4, \\
 (4) \quad \psi_{BSC} &= \mathbf{X}_1, \quad L_c = 3.9312, \quad \omega_c^2 = 1.0966, \quad \Delta\phi_c = \pi/4.
 \end{aligned} \tag{31}$$

Thus, in this description we have an important result that the BSC is simply one of the eigenmodes of the resonator coupled to the evanescent modes. For this eigenmode to be decoupled from the propagating channel of both waveguides the overlapping integrals

$$W_{j;01}^C = \psi_{01}(z = z_C) \psi_l(z_C) \int_0^{2\pi} d\alpha \int_0^1 \rho d\rho \vec{X}_j(r(\rho, \alpha), \phi(\rho, \alpha)), \quad C = L, R \tag{32}$$

have to be zero for selected $j = 1$ or $j = 2$. Fig. 16 demonstrates that the overlapping integral vanishes at the BSC points. Such BSCs form new class of the accidental BSCs [31, 33, 39]. Fig. 16 demonstrates that the BSC modes \vec{X}_j are twisted to have zero coupling on both interfaces. Again the BSCs occur on lines in the parametric space L and $\Delta\phi$ as shown in Fig. 17 by open circles. However there is the second line in which the BSC length L_c diverges when $\Delta\phi \rightarrow \pi/2$. Also it is important to note that the BSC modes do not support currents of acoustic intensity similar to the BSC 1 and 2.

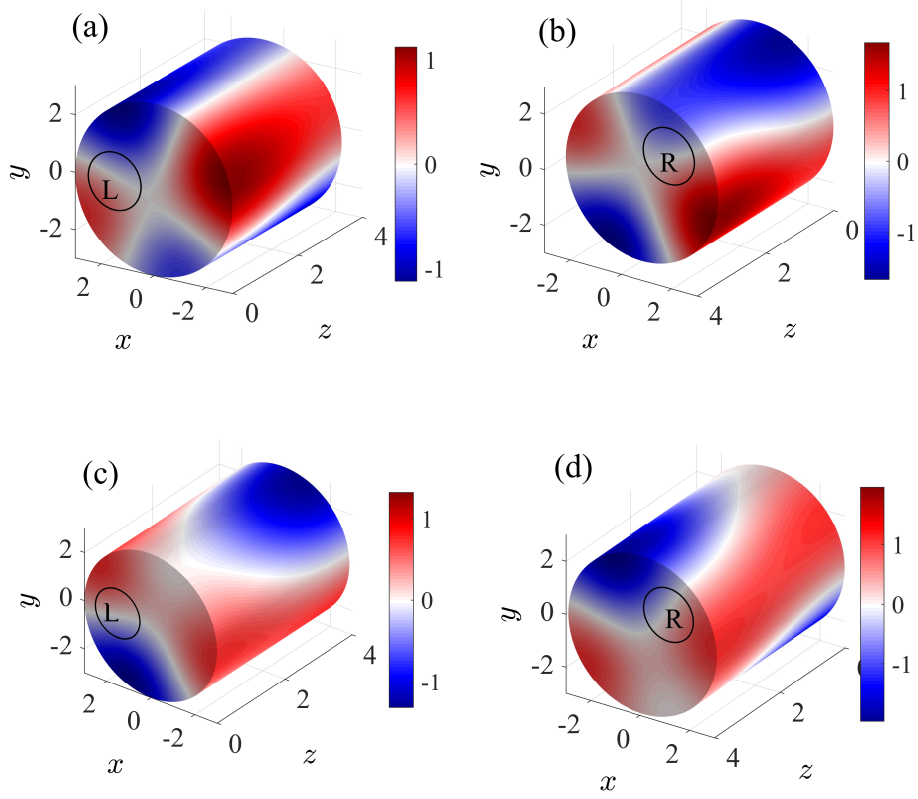


FIG. 16: (Color online) The real parts of the eigenmodes (30) of modified resonator. (a) and (b) \mathbf{X}_2 at the BSC point (3) (Eq. (31)) with side of input and output respectively. (c) and (d) the same for the \mathbf{X}_1 at the BSC point (4).

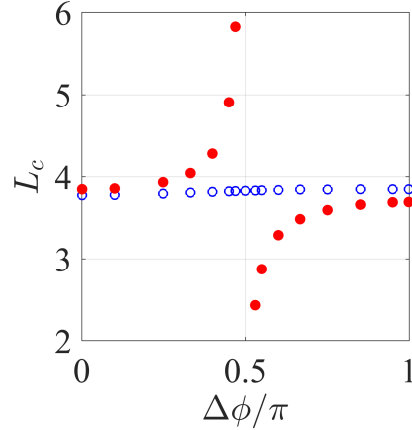


FIG. 17: (Color online) Lines of the BSCs in the parametric space of the resonator length and rotation angle $\Delta\phi$.

V. CONCLUSIONS

The method of the effective non-Hermitian Hamiltonian equivalent to the coupled mode theory [22] calculates the transmittance of waves through the resonator by Eq. (11). One can see that the shape of resonances and interference of them depends not only on the eigenfrequencies but also on the coupling matrix elements of the corresponding eigenmodes with propagating modes of the waveguides attached to the resonator. That effect was first experimentally

demonstrated by Rotter *et al* [7] by change of the coupling strength with use of diaphragms between the waveguides and the resonator. In the present paper we propose the path through which the coupling matrix elements do not change the strength but acquire only phase factors by simple means of rotation of input waveguide relative to the resonator. Other words, that transforms phase of the continua of the waveguide and can be performed in a realistic acoustic or electromagnetic experiment by the use of piston-like hollow-stem waveguides tightly fit to the interior boundaries of a cylindrical cavity [6] as shown in Fig. 1. Our numerical and analytical calculations have shown that simple setup cardinally effect Fano resonances that in turn opens and closes wave transmittance by small rotation to be claimed as the wave faucet.

Rigorously speaking rotation of one waveguides in a way shown in Fig. 1 the number of continua is doubled at $\Delta\phi \neq 0$. The problem of the BSC residing in a finite number of continua was considered in Ref. [28] in the framework of the Weisskopf-Wigner model [29]. Rigorous statement about the BSCs was formulated as follows. The interference among N degenerate states which decay into K non-interacting continua generally leads to the formation of $N - K$ BSCs. The equivalent point of view is that the linear superposition of the N degenerate eigenmodes can be achieved to have zero coupling with K different continua in $N - K$ ways by a variation of the N superposition coefficients a_n [?]. In particular if waveguides were attached at different radiuses the BSC would need in triple degeneracy of eigenlevels. However in the present case of rotation of one of the waveguides attributes only the phase factor $\exp(im\Delta\phi)$ to the coupling matrix elements of resonator with the left continua as was derived in Eq. (9). That allowed to avoid problem of triple degeneracy of resonator eigemodes. Moreover it gave rise to surprisingly rich variety of BSCs and respectively collapses of Fano resonances.

Off-center attachment of waveguides lifts a degeneracy of eigenmodes of the closed cylindrical resonator relative to sign of OAM given by integer m . As result the BSC is realized in the vicinity degeneracy of eigenlevels modified by evanescent modes with definite m and mode $m = 0$. Respectively the BSC expanded over the eigenmodes of closed resonator holds different contributions of m and $-m$ as explicitly given for example in Eq. (23).

To be specific we consider the case of acoustic wave transmission with the Neumann BCs but similar consideration can be performed for electromagnetic wave transmission with the Dirichlet BCs.

Acknowledgement: This work has been supported by RFBR through Grant 17-02-00440. A.S. acknowledges H. Schanz, P. Seba, L. Sirko and H.-J. Stöckmann for encouraging discussions. The authors thank D.N. Maksimov for helpful discussions.

-
- [1] Thomas Young, "Bakerian Lecture: Experiments and calculations relative to physical optics", *Phil. Trans. Royal Soc.* **94**, 116 (1804). doi:10.1098/rstl.1804.0001.
 - [2] J. Von Neumann and E. Wigner, "Über merkwürdige diskrete eigenwerte", *Z. Phys* **30**, 467 (1929).
 - [3] Y. Aharonov and D. Bohm, "Significance of Electromagnetic Potentials in the Quantum Theory", *Phys. Rev.* **115**, 485 (1959).
 - [4] U. Fano, "Effects of Configuration interactions on Intensities and Phase Shifts", *Phys. Rev.* **124**, 1866 (1961).
 - [5] J.F. Nye and M.V. Berry, "Dislocations in wave trains", *Proc. R. Soc. London, Ser.A* **336**, 165 (1974).
 - [6] A.A. Lyapina, D.N. Maksimov, A.S. Pilipchuk, and A.F. Sadreev, "Bound states in the continuum in open acoustic resonators," *J.Fluid Mech.* **780**, 370 (2015).
 - [7] S. Rotter, F. Libisch, J. Burgoffer, U. Kuhl, and H.-J. Stöckmann, "Tunable Fano resonances in transport through microwave billiards," *Phys. Rev.* **E69**, 046208 (2004).
 - [8] H. Friedrich and D. Wintgen, "Interfering resonances and bound states in the continuum," *Phys. Rev.* **A32**, 3231 (1985).
 - [9] A. Volya and V. Zelevinsky, "Non-Hermitian effective Hamiltonian and continuum shell model," *Phys. Rev.* **C67**, 054322 (2003).
 - [10] A.F. Sadreev, E.N. Bulgakov, and I. Rotter, "Bound states in the continuum in open quantum billiards with a variable shape," *Phys. Rev. B* **73**, 235342 (2006).
 - [11] R. Parker, "Acoustic resonances and blade vibration in axial flow compressors", *J. Sound and Vibration* **92**, 529 (1984).
 - [12] Y. Duan and M. McIver, "Rotational acoustic resonances in cylindrical waveguides", *Wave Motion* **39**, 261 (2004).
 - [13] Chia Wei Hsu, Bo Zhen, A.D. Stone, J.D. Joannopoulos and M. Soljačić, "Bound states in the continuum," *Nature Rev. Mat.* **1** (2016).
 - [14] A. Kodigala, T. Lepetit, Q. Gu, B. Bahari, Y. Fainman, and B. Kanté, "Lasing action from photonic bound states in continuum", *Nature* **541**, 196–199 (2017).
 - [15] ZH. Zhang, Y. Li, W. Liu, J. Yang, Y. Ma, H. Lu, Y. Sun, H. Jiang, "Controllable lasing behavior enabled by compound dielectric waveguide grating structures", *Opt. Express* **24**, 19458–19466 (2016).
 - [16] J.W. Yoon, S.H. Song, R. Magnusson, "Critical field enhancement of asymptotic optical bound states in the continuum," *Sci. Rep.* **5**, 18301 (2015).
 - [17] Mingda Zhang and Xiangdong Zhang, "Ultrasensitive optical absorption in graphene based on bound states in the continuum," *Sci. Rep.* **5**, 8266, (2015).

- [18] E.N. Bulgakov, A.F. Sadreev, and D.N. Maksimov, "Light Trapping above the Light Cone in One-Dimensional Arrays of Dielectric Spheres", *Appl. Sciences* **7**, 147 (2017).
- [19] E.N. Bulgakov, and D.N. Maksimov, "Light enhancement by dielectric arrays," arXiv preprint arXiv:1702.05990 (2017).
- [20] J. Okołowicz, M. Płoszajczak, and I. Rotter, "Dynamics of quantum systems embedded in a continuum," *Phys. Rep.* **374**, 271–383 (2003).
- [21] A.F. Sadreev and I. Rotter, "S-matrix theory for transmission through billiards in tight-binding approach," *J. Phys. A* **36**, 11413 (2003).
- [22] D. N. Maksimov, A. F. Sadreev, A. A. Lyapina, and A. S. Pilipchuk, "Coupled mode theory for acoustic resonators," *Wave Motion*, **56**, 52 (2015).
- [23] K. Pichugin, H. Schanz, and P. Seba, "Effective coupling for open billiards," *Phys. Rev. E* **64**, 056227 (2001).
- [24] I. Rotter and A. F. Sadreev, "Zeros in single-channel transmission through double quantum dots," *Phys. Rev. E* **71**, 046204 (2005).
- [25] V.V. Sokolov and V.G. Zelevinsky, "Dynamics and statistics of unstable quantum states," *Nucl. Phys. A* **504**, 562–588 (1989).
- [26] T. Lepetit and B. Kant'è, "Controlling multipolar radiation with symmetries for electromagnetic bound states in the continuum," *Phys. Rev. B* **90**, 241103(R) (2014).
- [27] P. J. Cobelli, V. Pagneux, A. Maurel, and P. Petitjeans, "Experimental study on water-wave trapped modes," *J. Fluid Mech.* **666**, 445 (2011).
- [28] F. Remacle, M. Munster, V.B. Pavlov-Verevkin and M. Desouter-Lecomte, "Trapping in competitive decay of degenerate states," *Phys. Lett. A* **145**, 265 (1990).
- [29] H. Feshbach, "Unified Theory of Nuclear reactions," *Ann. Phys. N.Y.* **5** 357 (1958).
- [30] E.N. Bulgakov and A.F. Sadreev, "Spin polarized bound states in the continuum in open AharonovBohm rings with the Rashba spinorbit interaction," *J. Phys.: Cond. Mat.* **28**, 265301 (2016).
- [31] E. Bulgakov and A. Sadreev, "Formation of bound states in the continuum for a quantum dot with variable width," *Phys. Rev. B* **83**, 235321 (2011).
- [32] Chia Wei Hsu, Bo Zhen, J. Lee , Song-Liang Chua, S.G. Johnson, J.D. Joannopoulos and M. Soljagic, "Observation of trapped light within the radiation continuum," *Nature* **499**, 188 (2013).
- [33] Bo Zhen, Chia Wei Hsu, Ling Lu, A.D. Stone, and M. Soljačić, "Topological Nature of Optical Bound States in the Continuum," *Phys. Rev. Lett.* **113**, 257401 (2014).
- [34] Yi Yang, Chao Peng, Yong Liang, Zhengbin Li, and S. Noda, "Analytical Perspective for Bound States in the Continuum in Photonic Crystal Slabs," *Phys. Rev. Lett.* **113**, 037401 (2014).
- [35] S. Hein, W. Koch and L. Nannen, "Trapped modes and Fano resonances in two-dimensional acoustical duct-cavity systems," *J. Fluid Mech.* **692** 257 (2012).
- [36] L. Xiong, W. Bi, and Y. Aurégan, "Fano resonance scatterings in waveguides with impedance boundary conditions," *J. Acoust. Soc. Am.* **139**, 764 (2016).
- [37] S. Hein and W. Koch, "Acoustic resonances and trapped modes in pipes and tunnels," *J. Fluid Mech.* **605**, 401 (2008).
- [38] C.S. Kim, A.M. Satanin, Y.S. Joe, R.M. Cosby, "Resonant tunneling in a quantum waveguide: Effect of a finite-size attractive impurity," *Phys. Rev. B* **60** 10962-10970 (1999).
- [39] A.S. Pilipchuk, A.F. Sadreev, "Accidental bound states in the continuum in an open Sinai billiard," *Phys. Lett. A* **381**, 720724 (2017).